Small-scale universality of particle dynamics in quantum turbulence

M. La Mantia,* P. Švančara, D. Duda, and L. Skrbek
Faculty of Mathematics and Physics, Charles University, Ke Karlovu 3, 121 16 Prague, Czech Republic
(Received 16 May 2016; revised manuscript received 7 November 2016; published 28 November 2016)

We show that, in turbulent two-fluid flows of superfluid ^{4}He, the statistically described dynamics of small particles suspended in the liquid does not depend on the type of imposed flow, at scales smaller than the average distance between quantized vortices, the quantum length scale of the flow. More precisely, regardless of the mechanically or thermally driven nature of the large-scale flow, the tails of the observed particle velocity statistical distributions, indicating the occurrence of large-magnitude events in the proximity of quantized vortices, display the same power-law shape, characteristic of the quantum description of superfluid ^{4}He. This property of quantum turbulence can be linked to the small-scale universality observed in classical turbulent flows of viscous fluids.

DOI: 10.1103/PhysRevB.94.184512

I. INTRODUCTION

Properties of natural systems often depend on the scale at which they are investigated. Systems that appear similar at a certain scale may look entirely different at another scale, leading to the possibility of discovering hidden connections between apparently dissimilar phenomena. In other words, the same bricks can be used to build different houses or, similarly, the same house can be built by using different bricks. We apply this research approach to the study of quantum turbulence [1–3], which can loosely be defined as the most general form of motion of quantum fluids displaying superfluidity, and we specifically focus on turbulent flows of superfluid ^{4}He, known as He II, above 1 K. On the phenomenological level, this quantum fluid is viewed as consisting of two interpenetrating fluids. The gas of thermal excitations—the viscous normal component—carries the entire entropy content of the quantum fluid, while the superfluid component is assumed inviscid and its circulation is quantized in units of the circulation quantum $\kappa = h/m = 9.97 \times 10^{-8}$ m^2/s, where h is the Planck constant and m denotes the mass of the ^{4}He atom [4].

Singly quantized vortices, usually arranged in a tangle, may exist in He II. In the zero-temperature limit, where there is no normal fluid, the vortex tangle dynamics represents the simplest prototype of turbulence. At finite temperature (as in the present study) turbulence may also occur in the viscous normal fluid and be influenced by the mutual friction force arising from the scattering of thermal excitations by the quantized vortices [1–3]. Quantum turbulence may therefore bring to light challenging problems, unknown in its classical counterpart [5–11].

The interpretation of recent visualization results led to the conclusion that, at length scales larger than the quantum length scale ℓ_q of the probed flow, defined as the average distance between quantized vortices, turbulent He II behaves as if it were a viscous fluid, while its quantum nature becomes apparent at smaller scales. More precisely, in thermal counterflow (a thermally generated quantum flow with no obvious classical analog), the velocity and acceleration distributions of small particles suspended in the liquid have, at large enough scales, classical-like shapes, while, at scales smaller than ℓ_q, they are characterized by power-law tails emerging from the quantum description of He II [6,7]. So, it was indeed proven that the same house can be built by using different bricks.

Here we show that the same bricks can be used to build different houses. We investigate experimentally, by visualization, the flow-induced dynamics of relatively small particles in thermally and mechanically driven flows of superfluid ^{4}He, which appear distinctly different at scales larger than ℓ_q. Still, if the probed length scale ℓ_{exp} is smaller than ℓ_q, we find that the tails of the particle velocity distributions (which indicate the occurrence of rare events of large magnitude) are nearly identical, in the range of investigated parameters. Our experimental result therefore supports the long-held expectation that, at small enough length scales, the dynamics of quantized vortices does not depend on the type of imposed large-scale flow. Additionally, this property of quantum turbulence can be seen as analogous to the small-scale universality observed in classical turbulent flows of viscous fluids, see, e.g., Refs. [12–15], as it emerges from the pioneering work of Kolmogorov [16,17].

Fundamental results in the study of quantum flows have been obtained by visualizing the dynamics of solid hydrogen or deuterium particles of micrometer size, see Ref. [18] and references therein. Their motion is complex, as particles interact with both the normal and superfluid velocity fields simultaneously, and may become trapped (and/or detrapped) onto the cores of quantized vortices (it is consequently not straightforward to separate, in the range of investigated parameters, the contributions to the particle dynamics originating independently from the two postulated flow fields; see Ref. [19] for a detailed discussion). Nevertheless, the visualization of flows of superfluid ^{4}He, seeded with these particles, resulted in the discovery of nonclassical velocity [5,6,20] and acceleration [7,21] statistics in thermal counterflow, among other results, such as observations of quantized vortex reconnections [22], Kelvin waves [23], mechanically driven flows past a circular cylinder [24], and due to an oscillating rectangular cylinder [25].

We extend these investigations by using the Prague cryogenic setup, described in detail in our previous publications [6,7,19–21,25,26], and report here results obtained by visualizing particle dynamics in three different quantum flows, in various experimental conditions, and by probing

*lamantia@nbox.troja.mff.cuni.cz

experimentally these flows at length scales straddling two orders of magnitude across the quantum length scale ℓ_q of the flow: (i) thermal counterflow in the bulk, as far away as possible from fluid boundaries [6,7], (ii) thermal counterflow in the proximity of a wall, approximately ten times closer to the fluid boundary than in the previous case, and (iii) flow due an oscillating cylinder, which is a mechanically driven flow [25].

The main difference between thermally and mechanically driven flows of He II is that, in thermal counterflow, the normal and superfluid components flow, on average, in opposite directions, while, for mechanically generated flows, the two components are, at large enough length scales, locked together and move, on average, in the same direction; for a detailed discussion, see, for example, Ref. [27]. Our experimental results show that, at small enough flow scales, $\ell_{exp} < \ell_q$, this difference disappears and that the particle motions, when statistically described, appear to be influenced only by the quantized vortex dynamics, independently of the imposed mean flow.

Additionally, the role of solid boundaries in quantum flows is yet to be investigated in detail, as to date only a few studies have addressed the issue and solely at scales larger than ℓ_q [8,27–35]. We report how particles in thermal counterflow behave close to a solid wall, at flow scales smaller that those probed previously. Our aim is to contribute to this emerging line of enquiry in quantum turbulence research (boundary effects on classical flows are extensively studied, see, e.g., Ref. [36] and references therein).

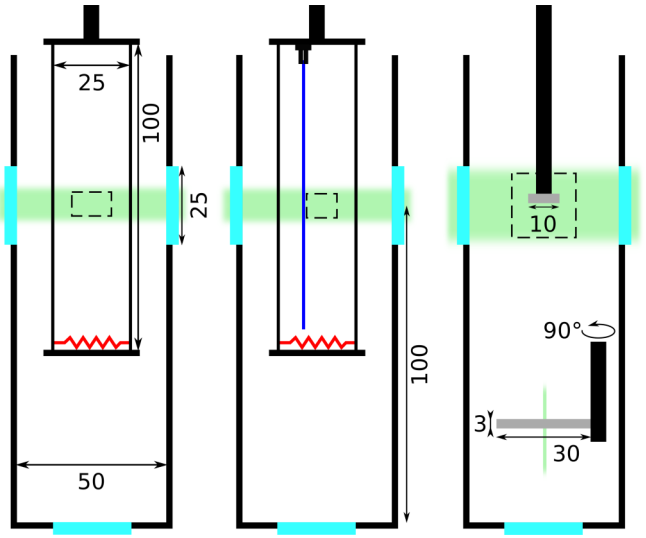

FIG. 1. Sketches of the three different flow generators (dimensions in mm; see the main text for further details). Only the bottom part of our experimental volume (the innermost part of the cryostat optical tail) is shown, for the sake of clarity (the cyan rectangles represent three of the five tail optical ports). The laser sheet, perpendicular to the camera, is depicted in green, while the camera field of view is indicated by the black dashed line. The red line represents the flat heater, placed on the bottom of the counterflow glass channel (displayed in black). Left: bulk counterflow. Middle: counterflow in the proximity of a wall (dark blue line). Right: the oscillating cylinder (shown in gray) is attached to a metallic shaft (black); a perpendicular view of the cylinder is displayed at the bottom of the sketch.

II. METHODS

The experimental technique we use is based on visualizing the motions of relatively small particles suspended in the liquid, their size being smaller than (or of the same order of) relevant flow scales. The particles are generated by mixing helium and hydrogen (or deuterium) gasses at room temperature, in a volume ratio of approximately 100 to 1, and by injecting the mixture into the helium bath (gaseous hydrogen, or deuterium, solidifies during the injection). The imposed flow induces the particles to move and, since they reflect the light of a laser sheet, their time-dependent positions are captured by a fast digital camera, which is situated perpendicularly to the thin (less than 1 mm thick) laser sheet and is sharply focused on the illuminated plane by using an appropriate macro lens (the camera and laser are outside the experimental volume, at room temperature; see Refs. [19,20] for schematic views of the setup).

Thermal counterflow experiments are performed in a vertical glass channel of square cross section, of 25 mm sides, and 100 mm long (a flat heater is placed on the channel bottom to generate the flow; see Ref. [19] for a picture of the channel and Fig. 1 for relevant sketches). The 1 Mpx CMOS camera field of view is, for the bulk experiments, 13 mm wide and 8 mm high, and is situated as far as possible from the flow boundaries [6,7], that is, the channel walls are about 6 mm away from the field of view vertical sides (the field of view is in the middle of the channel). For the experiments in the proximity of a solid boundary, an additional glass wall (75 mm long, 25 mm wide, and 1 mm thick) is inserted inside the channel. Here, the camera field of view is 10 mm wide and 8 mm high, and its left side (that farther from the laser) is 0.6 mm away from the additional wall, that is, ten times closer to the solid boundary than in the case of the bulk counterflow experiments (the distance between the right side of the field of view and the glass channel wall is 6 mm, as above).

The strength of this thermally driven flow is quantified by the counterflow velocity

$$v_{ns} = v_n - v_s = \frac{q}{\rho S T}\left(1 + \frac{\rho_n}{\rho_s}\right) = \frac{q}{\rho_s S T}, \qquad (1)$$

where v_n and v_s indicate the normal fluid and superfluid velocities, respectively; once the heater is switched on, the superfluid component moves toward the heat source and the normal component flows away from it, in order to conserve the null mass flow rate (we assume here that $v_n > 0$ and $v_s < 0$). The total density ρ of the fluid, defined as the sum of the densities of its normal (ρ_n) and superfluid (ρ_s) components, depends weakly on temperature, while the densities ρ_n and ρ_s display much stronger temperature dependencies (He II can be often considered entirely superfluid at temperatures below 1 K); q is the applied heat flux, S denotes the entropy per unit mass, tabulated, together with other fluid properties, in Ref. [4], and T indicates the temperature (liquid ^{4}He becomes superfluid below the transition temperature $T_\lambda \approx 2.17$ K, at the saturated vapor pressure; above T_λ it is a classical viscous fluid, known as He I).

The mechanically driven flows are obtained inside our experimental volume (of square cross section, of 50 mm sides, and 300 mm long) by vertically oscillating a transparent cylinder, of rectangular cross section (10 mm wide and 3 mm high; see Ref. [25] for relevant pictures and Fig. 1 for a sketch of the setup). The vertical laser sheet illuminates the middle part of the cylinder length (30 mm). The oscillation frequency f is set between 0.05 and 1.25 Hz, and the corresponding amplitude a is 5 or 10 mm (the cylinder oscillates in the middle part of the experimental volume, where its optical ports, of 25 mm diameter, are located, approximately 100 mm above the volume bottom). The camera field of view is 21 mm wide and 16 mm high, for $a = 5$ mm, and 21 mm wide and 21 mm high, for $a = 10$ mm; see Ref. [25] for further details.

Thermal counterflow movies are recorded at 400 fps, while oscillating cylinder movies are obtained at 100 fps. The images are collected at constant temperature, approximately one minute after the fluid is set into motion, in order to ensure that the investigated flows have reached a steady state. The particle positions and trajectories are calculated from the movies by using an open-source tracking algorithm [37]. Each movie is typically made of a few thousand images (in each image there are usually up to a few hundred particles) and several thousand trajectories, with up to a few hundred points, are computed for each movie. The obtained tracks are filtered by using dedicated computer programs, developed by us, in order to remove spurious trajectories before calculating the velocities, which are computed by interpolating linearly consecutive position differences. The distance between the particles along the trajectories, which can be seen as a measure of the probed length scale, is proportional to the time between successive frames, i.e., it generally decreases as the frame rate increases. Besides, particle positions at a low frame rate can also be obtained by accordingly removing particle positions from data sets recorded at a high frame rate, not only from images recorded at a low frame rate [6,7]. The Lagrangian quantities calculated from several movies obtained under the same conditions are finally combined.

III. LENGTH SCALES

The smallest length scale ℓ_{exp} probed in our experiments is the particle size, of the order of a few micrometers, see Ref. [6] for typical particle size distributions. However, if the images are not taken fast enough, it may occur that a particle travels a distance larger than its size between two consecutive images. We therefore define the ratio $R = \ell_{\mathrm{exp}}/\ell_{\mathrm{q}}$ between the length scale probed by the particles (larger than or of the same order of the average particle size) and the quantum length scale of the investigated flow (that is, the average distance between quantized vortices). As detailed below, we obtain values of ℓ_{exp} straddling about two orders of magnitude across ℓ_{q}, that is, R results always larger than 0.01 and lower than 100.

In the case of the thermal counterflow experiments, we set $\ell_{\mathrm{exp}} = V_{abs}t_1$, where V_{abs} denotes the average particle velocity, obtained at the smallest time between particle positions, and t_1 indicates the time between two consecutive particle positions, used for the calculation of the velocities [6,7]. The corresponding ℓ_{q} is computed as detailed in Ref. [6], i.e., by using relevant published data [38].

More precisely, in the present conditions, i.e., at large enough heat fluxes, the imposed counterflow generates a tangle of vortex line density $L \approx \gamma(T)^2 v_{ns}^2$, where the parameter $\gamma(T)$ is known with sufficient accuracy (of about 30%, see, e.g., Ref. [39] and references therein). We therefore experimentally select the quantum length scale $\ell_{\mathrm{q}} \approx 1/\sqrt{L}$, by tuning the heat flux q, and, following our previous works [6,7], we use the values of $\gamma(T)$ reported in Ref. [38] to estimate the average distance ℓ_{q} between quantized vortices.

For the oscillating cylinder flows, we set the length scale ℓ_{exp} probed by the particles equal to $2\pi f a t_1$. In order to estimate the corresponding ℓ_{q} we make a few additional assumptions and, as a first step, on the basis of the results of our previous work [25], we take the definition of the Kolmogorov dissipative scale $\eta = (\nu^3/\varepsilon)^{1/4}$ [16], where ν is the fluid kinematic viscosity and ε indicates the mean dissipation rate of the flow. The latter, in turbulent flows of viscous fluids, can be set equal to $\nu\Omega^2$, where Ω is the average flow vorticity, which is calculated from the spatial derivatives of the fluid velocity and can be seen as a measure of the flow strength; consider also that, at scales larger than (or of the order of) η, the related flow behavior is expected to be universal, see, e.g., Refs. [12–17].

The following step is to assume that Ω^2 is approximately equal to the ensemble average of the experimentally obtained parameter θ^2, which is computed by taking suitably into account the spatial distribution of the particle velocities and their magnitudes in the proximity of the oscillating cylinder, see Ref. [25] for further details. We can now write that

$$\ell_{\mathrm{q}} \approx \eta \approx \left(\frac{\nu^2}{\langle\theta^2\rangle}\right)^{1/4}, \tag{2}$$

i.e., we assume that, for the studied oscillating cylinder flows, the average distance ℓ_{q} between quantized vortices is approximately equal to the length scale obtained by adequately applying the definition of the Kolmogorov length scale to flows of He II.

For He I, which is a viscous fluid, ν is tabulated in Ref. [4]. The values of the effective kinematic viscosity of turbulent He II reported in the literature (see, for example, Ref. [27] and references therein) are, in the investigated range of temperatures, of the same order of magnitude of the kinematic viscosity value of He I just above T_λ, that is, $\nu = 1.66 \times 10^{-8}$ m^2/s [4], which can also be expressed as $\kappa/6$ [25]. Hence, for the sake of simplicity and consistency with our previous work [25], in order to estimate from Eq. (2) ℓ_{q} for the oscillating cylinder data obtained in He II, we set $\nu = \kappa/6$.

More generally, the just given length-scale definitions are based on several assumptions, whose main justification is that they lead to positive comparisons with experimental data, as shown below and in our previous publications [6,7,25]. However, the reader should not forget that they are indeed approximations, which are therefore not expected to capture entirely the physics of the problem.

Another quantity that can be used to characterize our data is the thickness of the layer close to the fluid boundary where viscous effects, if any, are deemed to be significant. For the oscillating cylinder data, it is possible to calculate the viscous

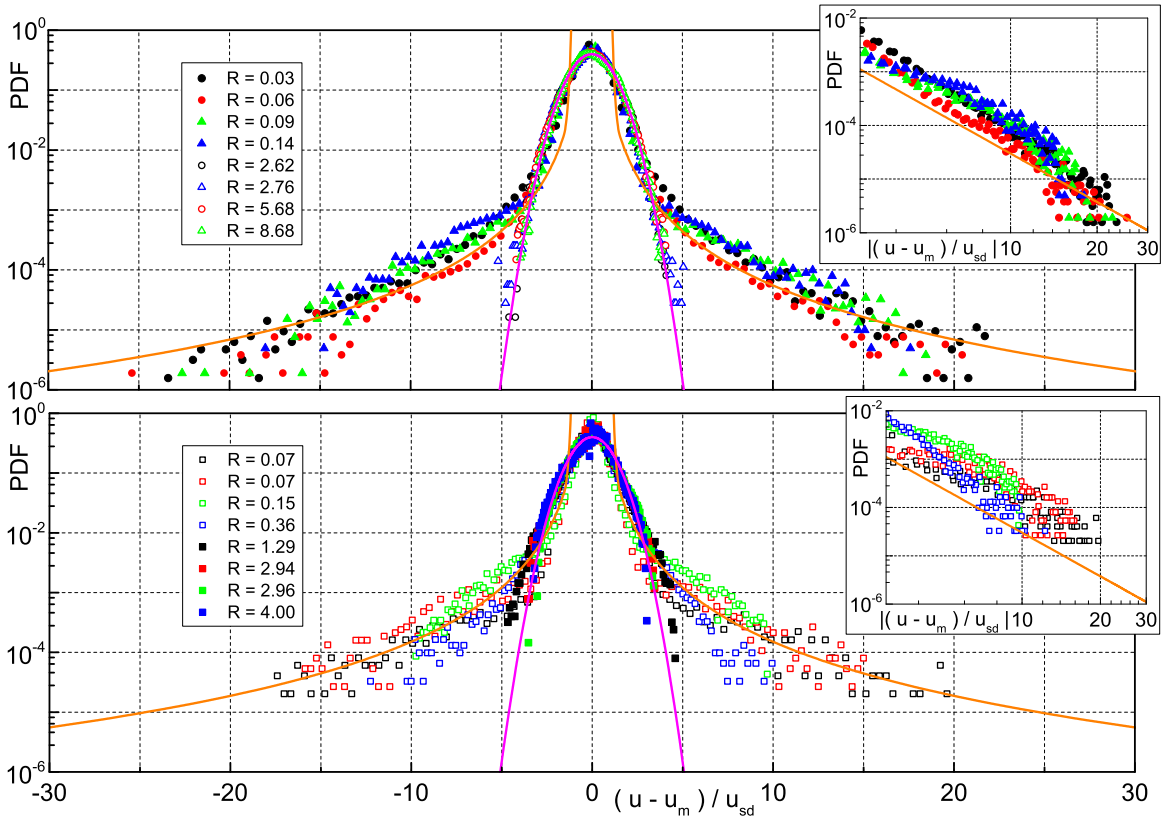

FIG. 2. Probability density function (PDF) of $(u - u_m)/u_{sd}$. Trajectories with at least five particle positions; total number of points: see the inset of Fig. 4; the area below the data curves is normalized to unity. Circles and triangles denote counterflow data obtained in the proximity of a wall and in the bulk, respectively, with $t_1 = 0.025$ s (filled symbols), $t_1 = 0.25$ s (open black and red circles, open green triangles), and $t_1 = 0.05$ s (open blue triangles). Black circles: $T = 1.95$ K, $q = 293$ W/m^2, $v_{ns} = 2.4$ mm/s, $V_{abs} = 1.5$ mm/s, $\ell_q = 145$ μm; red circles: $T = 1.95$ K, $q = 587$ W/m^2, $v_{ns} = 4.9$ mm/s, $V_{abs} = 1.7$ mm/s, $\ell_q = 73$ μm; green triangles: $T = 1.77$ K, $q = 612$ W/m^2, $v_{ns} = 6.8$ mm/s, $V_{abs} = 2.4$ mm/s, $\ell_q = 70$ μm; blue triangles: $T = 1.77$ K, $q = 608$ W/m^2, $v_{ns} = 6.8$ mm/s, $V_{abs} = 3.9$ mm/s, $\ell_q = 70$ μm, deuterium particles (the other data are obtained with hydrogen particles). Squares indicate oscillating cylinder data, with $t_1 = 0.01$ s and $a = 5$ mm: see the legend and Table I. Orange lines: power-law distributions, $C/|(u - u_m)/u_{sd}|^3$, to guide the eye, with C equal to 0.055 (top panel), 0.15 (bottom panel), and 0.03 (insets); magenta lines: Gaussian distributions. Insets: Log-log plots of the PDF of $|(u - u_m)/u_{sd}|$ for $R < 1$; symbols as in the main panels.

penetration depth, as discussed in Ref. [25]. We find that its numerical value is between 0.23 mm, for the smallest R, and 0.05 mm, for the largest R, that is, it is larger than the average particle size and of the same order of ℓ_q (computations performed assuming $\nu = \kappa/6$; in He I, the viscous penetration depth varies between 0.25 and 0.06 mm). For the thermal counterflow data, we can estimate the thickness of the viscous boundary layer by using the Blasius formula, which can be seen as an upper limit; see, for example, Ref. [40]. We find that its numerical value is about 2 mm. It follows that the bulk counterflow experiments are very likely not influenced by boundary effects, while the same cannot be said about the counterflow experiments in the vicinity of a wall, as the field of view is less than 1 mm away from the fluid boundary (calculations performed in the middle part of the channel, by using its hydraulic diameter).

IV. RESULTS AND DISCUSSION

Our main result is shown in Fig. 2, where the probability density function (PDF) of the dimensionless instantaneous particle velocity $(u - u_m)/u_{sd}$ in the horizontal direction is plotted. Here, u_m and u_{sd} indicate the mean value and the standard deviation of the dimensional velocity u, respectively (u is positive if directed from the left to the right of the field of view, toward the laser). Circles and triangles denote thermal counterflow data obtained in the proximity of a solid wall and in the bulk, respectively, and squares refer to the mechanically driven flow data (see the caption of Fig. 2 and Table I for the experimental conditions).

It is apparent that, at large particle velocities, all distributions, regardless of the type of flow, have the same power-law shape. To date, this feature was only observed by Paoletti *et al.* [5], in decaying counterflow, and by us [6], in steady-state counterflow. In the case of solid particles, whose motions are generally influenced by the quantized vortex tangle and by both velocity fields, the outcome can be justified by considering that particles trapped onto vortices can probe the occurrence of vortex reconnections [5].

We observe the same shape also in mechanically driven flows, which, at large enough scales, are expected to display features different from those observed in thermally driven flows [27]. This strongly suggests that, at length scales smaller than the quantum scale of the flow, particle motions are mainly

TABLE I. Experimental conditions of the oscillating cylinder data obtained in He II, see Fig. 2, Fig. 3, and Fig. 4. Length scale ratio R; temperature T, [K]; frequency f, [Hz]; amplitude a, [mm]; quantum length scale ℓ_q, [μm]. R and ℓ_q are estimated from Eq. (2).

R	T	f	a	ℓ_q
0.07	1.24	0.05	5	235
0.07	1.50	0.05	5	226
0.15	1.26	0.1	5	216
0.36	1.26	0.2	5	175
0.90	1.42	0.2	10	139
1.29	1.24	0.5	5	122
2.94	1.73	1	5	107
2.96	1.24	1	5	106
4.00	1.73	1.25	5	98
7.13	1.38	1	10	88

influenced by quantized vortex dynamics (by using particles about ten times smaller than the average distance between quantized vortices, we can indeed access flow scales smaller than ℓ_q, when collecting images at a fast enough frame rate).

The width of the tails of the velocity distributions can be seen as due to the finite size of the particles. As mentioned in Ref. [6], the upper limit can be derived from the assumption that the vortex tension force, acting on a trapped (spherical) particle, is balanced by the Stokes drag force, leading to a maximum velocity, that is, the velocity threshold for the trapped particle to break free,

$$v_{\max} = \frac{\rho_s \kappa^2}{6\pi^2 \mu d} \ln\left(\frac{r}{\xi}\right), \tag{3}$$

where d indicates the particle diameter and $r = d/2$ is its radius; μ denotes the fluid dynamic viscosity, tabulated in Ref. [4], and $\xi \approx 1$ Å is the vortex core size; a similar formula was derived in Ref. [41]. More precisely, following Ref. [42], the vortex tension force due to two vortex strands attached to the trapped particle can be approximated as

$$F_{VT} = 2\frac{\rho_s \kappa^2}{4\pi} \ln\left(\frac{r}{\xi}\right), \tag{4}$$

and the Stokes drag force, exerted on the particle by the normal fluid flow and assumed here to be parallel to F_{VT}, can be written as

$$F_S = 6\pi \mu r (u_n - u_p), \tag{5}$$

where u_n is the normal fluid velocity, set to zero for the trapped particle, and u_p denotes the particle velocity (the particle is supposed to be smaller than relevant flow scales; see also Ref. [7] for further details on the particle equation of motion).

If, consistently with experimental results [6,7], we set d equal to 5 μm, we find that $v_{\max} = u_p$ varies between 18 mm/s (wall counterflow) and 27 mm/s (bulk counterflow) and these values correspond to about 15 u_{sd}, the experimentally obtained upper limit, above which the PDF tails deviate from the power-law shape; see the upper panels of Fig. 2 and Table II. The fact that the latter deviation does not occur sharply can be explained by taking into account the relatively wide particle size distributions [6,7] (if d is two times smaller, $v_{\max}$ becomes almost two times larger).

TABLE II. Relevant particle velocities, obtained as detailed in the text, for the $R < 1$ data plotted in Fig. 2 and Fig. 3. Flow type: wall counterflow (WCF), bulk counterflow (BCF), oscillating cylinder flow (OCF); length scale ratio R; temperature T, [K]; mean particle velocity u_m; particle velocity standard deviation u_{sd}; maximum velocity $v_{\max}$, estimated from Eq. (3); velocity before trapping occurs u_t, from Eq. (7); all velocity values are in mm/s.

Flow type	R	T	u_m	u_{sd}	$v_{\max}$	u_t
WCF	0.03	1.95	0.2	1.2	18.1	1.8
WCF	0.06	1.95	0.2	1.3	18.1	1.8
BCF	0.09	1.77	−0.3	1.6	26.8	2.6
BCF	0.14	1.77	0.5	1.9	26.8	2.6
OCF	0.07	1.24	−1.2	1.9	24.5	2.4
OCF	0.07	1.50	1.0	2.4	30.9	3.0
OCF	0.15	1.26	0.1	3.9	25.4	2.5
OCF	0.36	1.26	0.4	3.6	25.4	2.5

For the oscillating cylinder experiments, $v_{\max}/u_{sd}$ ranges approximately between 7 and 13, as it can be inferred from Table II. Considering that the corresponding data sets are noticeably smaller than in counterflow, see the inset of Fig. 4, the agreement with experimental data, as displayed in the lower panels of Fig. 2, is fairly good, although worse than in counterflow.

In order to estimate the lower limit of the tail width we proceed as follows, on the basis of the particle equation of motion [7,42]. We calculate the particle velocity just before trapping occurs. We assume that the only contribution to the fluid acceleration is due to the velocity field of a straight quantized vortex (perpendicular to the large-scale flow direction) and that the particle acceleration is null, that is, a particle velocity larger than that computed below should lead to particle trapping. We can then write that

$$\rho_s(1 + C)V \frac{D\boldsymbol{u_s}}{Dt} + \boldsymbol{F_S} = 0, \tag{6}$$

where C is the added mass coefficient, equal to 1/2 for a spherical particle, and $V = 4\pi r^3/3$ indicates the particle volume; r denotes the particle radius, which, in this case, is also equal to the distance between the particle and vortex core. The superfluid velocity u_s in the proximity of the vortex can be calculated as $\kappa/(2\pi r)$ and is equal to 6.3 mm/s, for $r = 2.5$ mm; the corresponding acceleration is $Du_s/Dt = -\kappa^2/(4\pi^2 r^3)$, where the negative sign indicates that it is directed toward the vortex core, that is, all particles (regardless of their density) are attracted to vortices also in the absence of viscosity [in Eq. (6) the velocity and force are vectors]. We finally obtain that the velocity before trapping occurs can be written as

$$u_t = \frac{\rho_s \kappa^2}{6\pi^2 \mu d} = u_n - u_p, \tag{7}$$

which is positive in the direction toward the vortex core.

In the case of thermal counterflow we can set $u_n = v_n$, see Eq. (1), and, if the particle is moving toward the straight vortex in the positive direction, i.e., from below, away from the heat source, in the normal fluid flow direction, we can say that the minimum particle velocity $v_{\min} = v_n + u_t$, as particles are attracted to vortices. We obtain that $v_{\min}/u_{sd}$ varies between

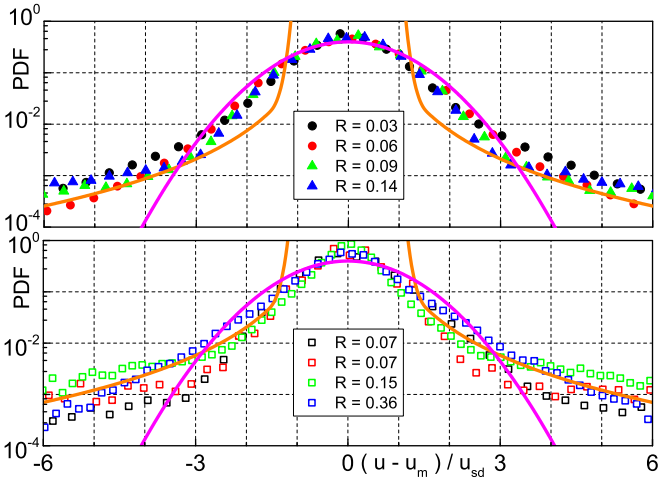

FIG. 3. PDF of $(u - u_m)/u_{sd}$ for $R < 1$ (core region); symbols as in the main panels of Fig. 2.

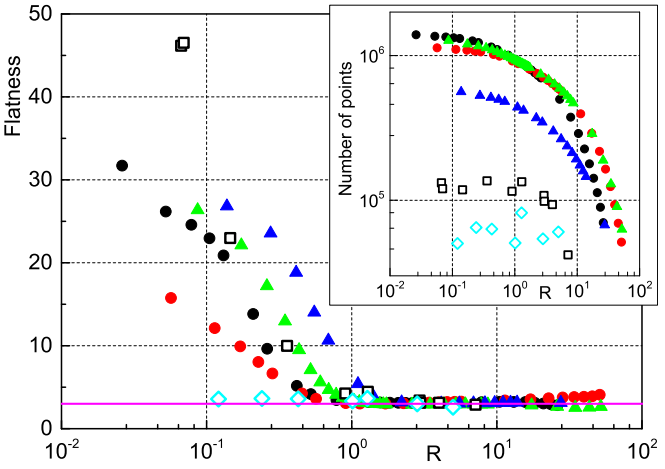

FIG. 4. Flatness of the $(u - u_m)/u_{sd}$ distribution as a function of R. Circles and triangles denote counterflow data obtained in the proximity of a wall and in the bulk, respectively, as in Fig. 2 (note, however, that the same symbols in Fig. 2 represent solely the data at the smallest R). Squares indicate oscillating cylinder data obtained in He II: see Table I. Diamonds denote oscillating cylinder data obtained in He I: see Table III. Magenta line: flatness of the Gaussian distribution. Inset: total number of particle positions as a function of R; symbols as in the main panel.

about 3 (wall counterflow) and 4 (bulk counterflow), the experimental obtained lower limit; see the upper panel of Fig. 3 and Table II.

For the mechanically driven flows, $u_n \approx 0$ and u_t/u_{sd} is approximately equal to 1, see Table II. In the lower panel of Fig. 3 it is indeed shown that the departure from the Gaussian shape possibly occurs at velocities smaller than in counterflow.

The reader should now take into account that the numerical values just reported can only be regarded as first-order estimates, due to the made assumptions. For example, we have considered straight stationary vortices, while actual quantized vortices do move within the two-component fluid and their topology is also affected by the attracted particles; see, for example, Ref. [42] and references therein. Additionally, we have previously shown that the shape of our particles is not necessarily spherical [20] and that particles do accelerate in thermal counterflow [7,21].

On the basis of these first-order estimates, we might argue that the particle velocity distributions (obtained in thermal counterflow) should display the power-law shape characteristic of quantum flows between about three and fifteen times the velocity standard deviation (assuming that the average particle size is 5 μm) and this is indeed what we see in Fig. 2 and Fig. 3. The same applies to the oscillating cylinder data sets, although, as noted above, the numerical values of the range extrema are slightly different.

Thus our experimental results can be explained as follows. The superfluid acceleration, due to the velocity field of the quantized vortices, is felt by the particles, also in the absence of viscosity, thanks to the inertial and added mass forces. Particles are then attracted to the vortices and can become trapped onto them. They can probe therefore the occurrence of vortex reconnections that is apparent from the shape of the particle velocity distributions. The fact that this is observed regardless of the imposed large-scale flow is the small-scale universality of particle dynamics we claim to observe in quantum turbulence.

We might add at this point that particle trapping is a dynamical process, that is, particles that become trapped onto vortices can be detrapped at a later time and vice versa, especially if the imposed large-scale flow is strong enough, as in the case of the present counterflow experiments; see, for example, Ref. [19] and references therein. We indeed observed that, at the values of heat flux considered here, most particles move away from the heater, in the direction of the normal fluid flow, and interact with the vortex tangle, as it is apparent from the fact that the corresponding particle tracks are not straight. Instead, at smaller heat fluxes, particle trajectories in the normal fluid flow direction appear straighter than those in the superflow direction, indicating therefore that, at values of q smaller than those considered here, particles tend to stay trapped onto vortices for longer times; see Ref. [19] for a detailed discussion.

The particle velocity distributions obtained from the oscillating cylinder data are clearly more scattered compared to those calculated from the counterflow experiments. This is likely due to the fact that the total number of particle positions obtained in the former case is about one order of magnitude smaller than those corresponding to the latter one, as displayed in the inset of Fig. 4. Nevertheless, the form of the oscillating cylinder distribution tails is consistent with the power-law shape expected in quantum flows, at small enough length scales.

The result, together with its just described explanation, is reinforced by the observation that, at large R, the particle velocity distributions are nearly Gaussian, as observed in classical flows, see, for example, Ref. [14] and references therein, regardless of the imposed flow type. Indeed, Fig. 4 displays the distribution flatness and it can be seen that, for R larger than 1, its value is around three, that of the Gaussian distribution; see also the shape of the particle distributions at large R in Fig. 2.

At small length scales ($R < 1$) the velocity distribution flatness depends on the type of flow, although, as displayed in

TABLE III. Experimental conditions of the oscillating cylinder data obtained in He I, see Fig. 4. Length scale ratio R; temperature T, [K]; frequency f, [Hz]; amplitude a, [mm]; dissipative length scale η, [μm]. R and η are estimated from Eq. (2).

R	T	f	a	η
0.12	2.26	0.05	5	130
0.24	2.26	0.1	5	131
0.43	2.27	0.2	5	147
1.01	2.19	0.2	10	124
1.28	2.27	0.5	5	123
2.83	2.18	0.5	10	109
4.99	2.18	0.75	10	94

Fig. 2, the tails have the same power-law shape. This can be linked to the fact that the flatness of a statistical distribution is mainly determined by large-magnitude events, which are indeed rare, that is, flatness is unlikely an adequate quantity to describe our experimental results at small scales. We expect, however, that for large enough data sets, substantially larger than the present ones, the same (universal) flatness behavior should be observed at low R, when particle motions are influenced solely by the vortex tangle dynamics, as shown by the power-law form of the velocity distribution tails.

Nevertheless, the calculation of the velocity distribution flatness at various length scales can be useful to estimate the average distance between quantized vortices, the quantum length scale of the flow, if the latter is not already known. Such a scale should indeed be of the same order of the smallest scale at which the value of the distribution flatness becomes approximately equal to three, as seen in Fig. 4. In other words, visualization studies are capable of giving results that are usually obtained by other means, such as the second sound attenuation technique (see, e.g., Ref. [27] and references therein).

Additionally, as a consistency check, the flatness values calculated for the investigated flows of He I (which is a viscous liquid) do not appear to depend on R (see Table III for the experimental conditions). The particle velocity distributions have quasi-Gaussian form at all scales, including those smaller than the dissipative scale η. To the best of our knowledge, this statistical property of classical turbulent flows has not been reported previously, likely due to the facts that (i) such small scales are difficult to probe experimentally in flows of viscous fluids, such as water or air, and that (ii) the flow behavior, at $\ell_{\rm exp} < \eta$, is not expected to be universal. However, this result is not the focus of the present work and further investigations should be performed to address the issue in detail.

If we look more closely at Fig. 2, we find that the distributions obtained in the proximity of a wall are slightly different from those calculated in the bulk, that is, it seems that the tails of the latter are wider than those of the former. Moreover, the flatness values for the present counterflow experiments close to a wall are smaller than those calculated from the bulk counterflow data, see Fig. 4. The outcome seems to be consistent with the physical picture emerging from recent studies on boundary effects in thermal counterflow [8,27,29–34], which suggest that, in the proximity of fluid boundaries, quantized vortices are, on average, closer to each

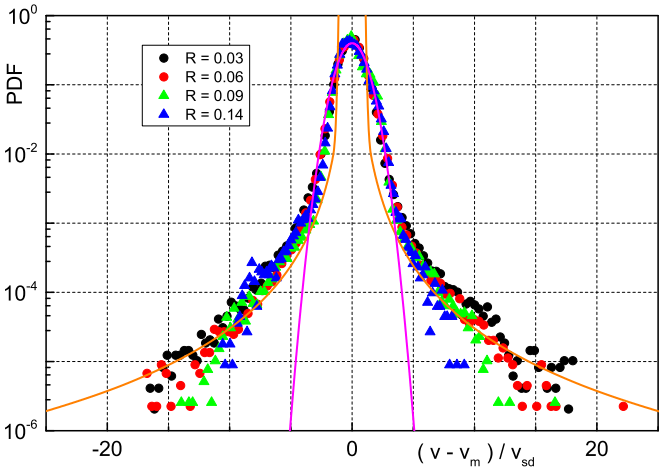

FIG. 5. PDF of $(v - v_m)/v_{sd}$. Circles and triangles denote counterflow data obtained in the proximity of a wall and in the bulk, respectively, as in Fig. 2. Orange line: power-law distribution, $0.03/|(v - v_m)/v_{sd}|^3$, to guide the eye. Magenta line: Gaussian distribution.

other than in the bulk, leading therefore to a larger effective R. A detailed account of the influence of solid boundaries on particle dynamics in thermal counterflow (including the corresponding velocity difference distributions) will be reported elsewhere.

The discussion above is mostly based on the statistical analysis of the particle velocities in the horizontal direction because the latter is perpendicular to the preferential direction of motion of the imposed flows. It is therefore easier to highlight our findings in the flow direction that, on average, is less influenced by the large-scale flow. Still, if we plot the PDF of the dimensionless instantaneous velocity $(v_s - v_m)/v_{sd}$ in the vertical direction, as shown in Fig. 5 (v_s and v_{sd} are the mean and standard deviation of the dimensional velocity v, respectively), we obtain the same power-law shape of the distribution tails (the oscillating cylinder data are more scattered but do not show a different power-law behavior at large enough velocities).

A closer look at Fig. 5 confirms that the vertical velocity distribution cores are in general characterized by a broad peak, which is often also skewed. This peak is most likely due to the existence of two velocity fields in steady-state thermal counterflow [5,6,19,20], while, for the mechanically driven flows, it can be linked to the shedding of large-scale vortical structures at the cylinder edges [25] (the latter feature can also be seen in the horizontal velocity distribution cores, as displayed in the bottom panel of Fig. 2). Note in passing that, to date, large vortical structures have not been extensively studied in thermal counterflow, although their existence is indirectly supported by a few experiments [7–11,43–45].

Finally, we note, once more, that the physical interpretation of our data is based on a number of assumptions, detailed above, which are not expected to capture entirely the physics of the problem. Nevertheless, these assumptions lead to consistent explanations, as, for example, at large enough length scales, $R > 1$, all particle velocity distributions have flatness values close to that of the Gaussian distribution, while, for $R < 1$, their shape does not depend on the type

of imposed large-scale flow, where R is obtained from the above mentioned assumptions. In other words, our work does not aim at answering all the questions related to particle-vortex interactions in He II but can be seen as a useful step toward a comprehensive understanding of this phenomenon.

V. CONCLUSIONS

We have shown that small-scale universality can be observed in quantum turbulence, similarly as in classical turbulence. Indeed, since postulated by Kolmogorov [16,17], a large number of related studies has been performed in the field of classical turbulence, see, e.g., Refs. [12–14] and references therein, including the recent numerical investigations showing that small-scale universality holds already in various flows of moderate Reynolds number [15].

However, in classical flows, these small scales are still larger than (or of the order of) the Kolmogorov length scale η, below which the fluid motion is dissipated into heat by the action of the fluid viscosity, while, in quantum flows, they are smaller than (or of the same order of) the quantum scale ℓ_q, the average distance between quantized vortices, below which fluid motion may exist all the way down to the Å scale, the size of the quantized vortex core. On the other hand, the behavior of classical flows at scales smaller than η, to the best of our knowledge, has yet to be studied in detail. This could be addressed by investigating, at suitable scales, other flows of liquid ^{4}He at temperatures larger than the superfluid transition, following Ref. [25]. Additionally, in both classical and quantum cases, it is assumed that the flow small scales are appreciably smaller than the large scales of the flow, which are of the order of the experimental volume size. In other words, the small-scale universality we observe can be seen as analogous to that reported to occur in classical flows, but has also different features.

A complementary view can perhaps be formulated as follows. It is generally accepted that in classical turbulence the departure from a purely Gaussian distribution of the velocity probability density function (or, in a more pronounced form, for the velocity difference) is due to intermittency effects, originating from rare events of large magnitude, possibly related to the fact that fluid tracers tend to lose energy faster than they gain it [46]. Quantized vortex reconnections may therefore play the role of such large-magnitude events in quantum turbulence and, consequently, the existence of the observed power-law tails in the velocity (and velocity difference) distributions could be linked to intermittency effects in classical flows.

Additionally, quantized vortices tend to move faster after reconnection than before it [47], and this time asymmetry could be seen as analogous to the one reported to occur in turbulent flows of viscous fluids [46]. Experimental evidence of the latter in quantum flows could possibly be obtained by using significantly smaller particles and by calculating higher order velocity statistics, but this is outside the scope of the present work and can be regarded as a suggestion for future studies. In any case, our statistical investigation of the motions of small particles in mechanically and thermally generated quantum flows of superfluid ^{4}He strongly suggests that the concept of small-scale universality might be a fruitful one for the deeper understanding of quantum turbulence as well as the phenomenon of fluid turbulence in general.

ACKNOWLEDGMENTS

We thank M. Rotter for valuable help and K. R. Sreenivasan and Y. Tsuji for useful discussions. We acknowledge the support of the Czech Science Foundation under Grant No. GAČR 16-00580S.

[1] W. F. Vinen and J. J. Niemela, Quantum turbulence, J. Low Temp. Phys. **128**, 167 (2002).
[2] L. Skrbek and K. R. Sreenivasan, Developed quantum turbulence and its decay, Phys. Fluids **24**, 011301 (2012).
[3] C. F. Barenghi, L. Skrbek, and K. R. Sreenivasan, Introduction to quantum turbulence, Proc. Natl. Acad. Sci. USA **111**, 4647 (2014).
[4] R. J. Donnelly and C. F. Barenghi, The observed properties of liquid helium at the saturated vapor pressure, J. Phys. Chem. Ref. Data **27**, 1217 (1998).
[5] M. S. Paoletti, M. E. Fisher, K. R. Sreenivasan, and D. P. Lathrop, Velocity Statistics Distinguish Quantum Turbulence from Classical Turbulence, Phys. Rev. Lett. **101**, 154501 (2008).
[6] M. La Mantia and L. Skrbek, Quantum, or classical turbulence?, Europhys. Lett. **105**, 46002 (2014).
[7] M. La Mantia and L. Skrbek, Quantum turbulence visualized by particle dynamics, Phys. Rev. B **90**, 014519 (2014).
[8] A. Marakov, J. Gao, W. Guo, S. W. Van Sciver, G. G. Ihas, D. N. McKinsey, and W. F. Vinen, Visualization of the normal-fluid turbulence in counterflowing superfluid ^{4}He, Phys. Rev. B **91**, 094503 (2015).
[9] J. Gao, A. Marakov, W. Guo, B. T. Pawlowski, S. W. Van Sciver, G. G. Ihas, D. N. McKinsey, and W. F. Vinen, Producing and imaging a thin line of He_2^* molecular tracers in helium-4, Rev. Sci. Instrum. **86**, 093904 (2015).
[10] J. Gao, W. Guo, V. S. L'vov, A. Pomyalov, L. Skrbek, E. Varga, and W. F. Vinen, The decay of counterflow turbulence in superfluid ^{4}He, JETP Lett. **103**, 648 (2016).
[11] S. Babuin, V. S. L'vov, A. Pomyalov, L. Skrbek, and E. Varga, Coexistence and interplay of quantum and classical turbulence in superfluid ^{4}He: Decay, velocity decoupling, and counterflow energy spectra, Phys. Rev. B **94**, 174504 (2016).
[12] K. R. Sreenivasan and R. A. Antonia, The phenomenology of small-scale turbulence, Annu. Rev. Fluid Mech. **29**, 435 (1997).
[13] F. Toschi and E. Bodenschatz, Lagrangian properties of particles in turbulence, Annu. Rev. Fluid Mech. **41**, 375 (2009).
[14] A. Tsinober, *An Informal Conceptual Introduction to Turbulence* (Springer, Berlin, 2009).
[15] J. Schumacher, J. D. Scheel, D. Krasnov, D. A. Donzis, V. Yakhot, and K. R. Sreenivasan, Small-scale universality in fluid turbulence, Proc. Natl. Acad. Sci. USA **111**, 10961 (2014).
[16] A. N. Kolmogorov, The local structure of turbulence in incompressible viscous fluid for very large Reynolds numbers, Dokl. Akad. Nauk. SSSR **30**, 299 (1941) [Proc. R. Soc. Lond. A **434**, 9 (1991)].

[17] A. N. Kolmogorov, Dissipation of energy in the locally isotropic turbulence, Dokl. Akad. Nauk. SSSR **32**, 19 (1941) [Proc. R. Soc. Lond. A **434**, 15 (1991)].
[18] W. Guo, M. La Mantia, D. P. Lathrop, and S. W. Van Sciver, Visualization of two-fluid flows of superfluid helium-4, Proc. Natl. Acad. Sci. USA **111**, 4653 (2014).
[19] M. La Mantia, Particle trajectories in thermal counterflow of superfluid helium in a wide channel of square cross section, Phys. Fluids **28**, 024102 (2016).
[20] M. La Mantia, T. V. Chagovets, M. Rotter, and L. Skrbek, Testing the performance of a cryogenic visualization system on thermal counterflow by using hydrogen and deuterium solid tracers, Rev. Sci. Instrum. **83**, 055109 (2012).
[21] M. La Mantia, D. Duda, M. Rotter, and L. Skrbek, Lagrangian accelerations of particles in superfluid turbulence, J. Fluid Mech. **717**, R9 (2013).
[22] G. P. Bewley, M. S. Paoletti, K. R. Sreenivasan, and D. P. Lathrop, Characterization of reconnecting vortices in superfluid helium, Proc. Natl. Acad. Sci. USA **105**, 13707 (2008).
[23] E. Fonda, D. P. Meichle, N. T. Ouellette, S. Hormoz, and D. P. Lathrop, Direct observation of Kelvin waves excited by quantized vortex reconnection, Proc. Natl. Acad. Sci. USA **111**, 4707 (2014).
[24] T. V. Chagovets and S. W. Van Sciver, Visualization of He II forced flow around a cylinder, Phys. Fluids **27**, 045111 (2015).
[25] D. Duda, P. Švančara, M. La Mantia, M. Rotter, and L. Skrbek, Visualization of viscous and quantum flows of liquid ^{4}He due to an oscillating cylinder of rectangular cross section, Phys. Rev. B **92**, 064519 (2015).
[26] D. Duda, M. La Mantia, M. Rotter, and L. Skrbek, On the visualization of thermal counterflow of He II past a circular cylinder, J. Low Temp. Phys. **175**, 331 (2014).
[27] E. Varga, S. Babuin, and L. Skrbek, Second-sound studies of coflow and counterflow of superfluid ^{4}He in channels, Phys. Fluids **27**, 065101 (2015).
[28] T. Xu and S. W. Van Sciver, Particle image velocimetry measurements of the velocity profile in He II forced flow, Phys. Fluids **19**, 071703 (2007).
[29] A. W. Baggaley and S. Laizet, Vortex line density in counter-flowing He II with laminar and turbulent normal fluid velocity profiles, Phys. Fluids **25**, 115101 (2013).
[30] L. Galantucci and M. Sciacca, Non-classical velocity statistics in counterflow quantum turbulence, Acta Appl. Math. **132**, 273 (2014).
[31] A. W. Baggaley and J. Laurie, Thermal counterflow in a periodic channel with solid boundaries, J. Low Temp. Phys. **178**, 35 (2015).
[32] S. Yui and M. Tsubota, Counterflow quantum turbulence of He-II in a square channel: Numerical analysis with nonuniform flows of the normal fluid, Phys. Rev. B **91**, 184504 (2015).
[33] L. Galantucci, M. Sciacca, and C. F. Barenghi, Coupled normal fluid and superfluid profiles of turbulent helium II in channels, Phys. Rev. B **92**, 174530 (2015).
[34] S. Yui, K. Fujimoto, and M. Tsubota, Logarithmic velocity profile of quantum turbulence of superfluid ^{4}He, Phys. Rev. B **92**, 224513 (2015).
[35] S. Ikawa and M. Tsubota, Coflow turbulence of superfluid ^{4}He in a square channel: Vortices trapped on a cylindrical attractor, Phys. Rev. B **93**, 184508 (2016).
[36] K. Avila, D. Moxey, A. de Lozar, M. Avila, D. Barkley, and B. Hof, The onset of turbulence in pipe flow, Science **333**, 192 (2011).
[37] I. F. Sbalzarini and P. Koumoutsakos, Feature point tracking and trajectory analysis for video imaging in cell biology, J. Struct. Biol. **151**, 182 (2005).
[38] Y. A. Sergeev, C. F. Barenghi, and D. Kivotides, Motion of micron-size particles in turbulent helium II, Phys. Rev. B **74**, 184506 (2006).
[39] S. Babuin, M. Stammeier, E. Varga, M. Rotter, and L. Skrbek, Quantum turbulence of bellows-driven ^{4}He superflow: Steady state, Phys. Rev. B **86**, 134515 (2012).
[40] H. Schlichting, *Boundary-Layer Theory* (McGraw-Hill, New York, 1979).
[41] T. V. Chagovets and S. W. Van Sciver, A study of thermal counterflow using particle tracking velocimetry, Phys. Fluids **23**, 107102 (2011).
[42] Y. A. Sergeev and C. F. Barenghi, Particles-vortex interactions and flow visualization in ^{4}He, J. Low Temp. Phys. **157**, 429 (2009).
[43] M. Murakami and N. Ichikawa, Flow visualization study of thermal counterflow jet in He II, Cryogenics **29**, 438 (1989).
[44] G. Stamm, F. Bielert, W. Fiszdon, and J. Piechna, Counterflow-induced macroscopic vortex rings in superfluid helium: Visualization and numerical simulation, Physica B **193**, 188 (1994).
[45] T. Zhang and S. W. Van Sciver, Large-scale turbulent flow around a cylinder in counterflow superfluid ^{4}He (He II), Nat. Phys. **1**, 36 (2005).
[46] A. Pumir, H. Xu, E. Bodenschatz, and R. Grauer, Single-Particle Motion and Vortex Stretching in Three-dimensional Turbulent Flows, Phys. Rev. Lett. **116**, 124502 (2016).
[47] S. Zuccher, M. Caliari, A. W. Baggaley, and C. F. Barenghi, Quantum vortex reconnections, Phys. Fluids **24**, 125108 (2012).